High-pressure thermodynamic, electronic and magnetic properties of Ni

2000 J. Phys.: Condens. Matter 12 8953

(http://iopscience.iop.org/0953-8984/12/42/302)

J. Phys.: Condens. Matter **12** (2000) 8953–8962. Printed in the UK PII: S0953-8984(00)16032-1

High-pressure thermodynamic, electronic and magnetic properties of Ni

Jianjun Xie†, S P Chen†, Holmann V Brand† and Ronald L Rabie‡

† Theoretical Division, Los Alamos National Laboratory, Los Alamos, NM 87545, USA
‡ Dynamic Experimentation Division, Los Alamos National Laboratory, Los Alamos, NM 87545, USA

Received 2 August 2000, in final form 18 September 2000

Abstract. The thermodynamic, electronic and magnetic properties of Ni at high pressures have been calculated using the *ab initio* pseudopotential plane-wave method and the density-functional theory. The *P–V–T equation of state* is obtained from the Helmholtz free energy of the crystal in the quasiharmonic approximation. The pressure dependence of the thermal expansion coefficient, bulk modulus, electronic band structure, phonon spectrum and the magnetic moment are presented. The calculated results are in good agreement with the available experiment measurements.

1. Introduction

High-pressure study of solids is of both practical and theoretical importance. The development of high-pressure techniques such as piston–cylinder, diamond-anvil-cell (DAC) and shock-wave methods [1–3] enables us to measure the pressure dependence of a lot of material properties. In high-pressure studies, the accuracy of the pressure measurement is determined by the precision of the pressure calibration. Most pressure gauges work precisely for pressures below 10 GPa. When the pressure goes higher, there is considerable uncertainty about the absolute accuracy of the high-pressure measurement [4]. The change in the unit-cell volume of a high-symmetry solid is a good measure of the pressure applied to the solid up to several hundreds of GPa. Once the P–V–T relationship, i.e., the *equation of state* (EOS), for a given material is known, an accurate pressure scale can be obtained. In order to predict the EOS in the high-pressure domain, a lot of theoretical models [5] have been proposed. These EOS models use the available low-pressure data such as the volume V_0, the isothermal bulk modulus B_0 and its pressure derivatives B_0' and B_0'' as inputs to predict the high-pressure behaviours of materials. However, the validity of these semi-empirical EOSs needs to be checked by acquiring more experimental data or by first-principles calculations.

The development of first-principles electronic structure calculations based on density-functional theory (DFT) provides an effective tool for studying the zero-temperature energetics of many systems. This method has been widely extended to finite-temperature studies by including the phonon contributions to the free energy of the crystal. There are a number of ways to study the thermodynamic properties of solids within the framework of DFT. One approach is that of *ab initio* constant-pressure molecular dynamics [6, 7] in which the thermal properties can be evaluated by statistically averaging over all dynamical configurations. An alternative approach is to calculate the free energy using the *ab initio* lattice dynamics in the quasiharmonic approximation [8]. In this approximation, the Helmholtz free energy is calculated by adding a

0953-8984/00/428953+10$30.00

dynamical contribution to static lattice total energy. The *dynamical* contribution is nowadays conveniently calculated by using the density-functional perturbation theory (DFPT) [9, 10]. Anharmonic effects are included through the explicit volume dependence of the vibrational frequencies. Calculations based on various semi-empirical models [11–14] as well as on first-principles methods [15–20] demonstrate that the quasiharmonic approximation provides a reliable description of the dynamic properties of many bulk materials below the melting point.

In this study, we apply the quasiharmonic approximation to the study of the pressure dependence of the thermodynamic, electronic and magnetic properties of nickel which is a ferromagnetic 3d transition metal. The first-principles EOS is constructed from the Helmholtz free energy. The thermal expansion coefficient and bulk modulus are then calculated at different pressures and temperatures. The pressure dependence of the electronic structure, phonon spectrum as well as the magnetic moment are presented.

2. Computational method

For a given temperature T and a volume V, the Helmholtz free energy of a crystal can be expressed in the quasiharmonic approximation as [21]

$$F(V,T) = E(V) + F_{\rm vib}(\{\omega(V)\},T) \equiv E(V) + k_{\rm B}T\sum_{\boldsymbol{q}}\sum_{j}\ln\left\{2\sinh\left(\frac{\hbar\omega_j(\boldsymbol{q})}{2k_{\rm B}T}\right)\right\} \tag{2.1}$$

where E is the *static* contribution to the internal energy—which is easily accessible by means of standard DFT calculations, F_{vib} represents the vibrational entropy contribution to the free energy and $\omega_j(\boldsymbol{q})$ is the frequency of the jth phonon mode at the wave vector $\boldsymbol{q}$ in the Brillouin zone (BZ). The volume dependence of $\omega_j(\boldsymbol{q})$ can be accurately obtained from the parameter-free *ab initio* calculations of the DFPT [9, 10].

The EOS is constructed as

$$p(V,T) = -\left(\frac{\partial F}{\partial V}\right)_T = -\frac{\partial E}{\partial V} - \frac{\partial F_{vib}}{\partial V} = -\frac{\partial E}{\partial V} + \frac{1}{V}\sum_{\boldsymbol{q}}\sum_{j}\gamma_j(\boldsymbol{q})\mathcal{E}(\omega_j(\boldsymbol{q})) \tag{2.2}$$

where $\gamma_j(\boldsymbol{q})$ is the Grüneisen parameter corresponding to the $(\boldsymbol{q}, j)$ phonon mode, defined as

$$\gamma_j(\boldsymbol{q}) = -\frac{\partial\omega_j(\boldsymbol{q})}{\partial V}\frac{V}{\omega_j(\boldsymbol{q})} \tag{2.3}$$

and $\mathcal{E}(\omega_j(\boldsymbol{q}))$ is the mean vibrational energy of the $(\boldsymbol{q}, j)$ phonon given by

$$\mathcal{E}(\omega_j(\boldsymbol{q})) = \hbar\omega_j(\boldsymbol{q})\left[\frac{1}{2} + \frac{1}{\exp(\hbar\omega_j(\boldsymbol{q})/k_BT) - 1}\right]. \tag{2.4}$$

The thermal expansion at a given temperature and pressure is obtained directly from the EOS (2.2) and the volume thermal expansion coefficient is defined as

$$\alpha_V = \frac{1}{V}\left(\frac{\partial V}{\partial T}\right)_P. \tag{2.5}$$

The temperature dependence of the bulk modulus is obtained from

$$B(T) = V\left(\frac{\partial^2 F}{\partial V^2}\right)_T = V\frac{\partial^2 E}{\partial V^2} + V\left(\frac{\partial^2 F_{vib}(\{\omega(V)\},T)}{\partial V^2}\right)_T. \tag{2.6}$$

The static total energy $E(V)$ and the volume-dependent phonon frequencies $\omega_j(\boldsymbol{q})$ in the above equations are calculated by using DFT and DFPT respectively, with the generalized gradient approximation (GGA) [22] to the exchange–correlation functional. The interaction

between the valence electrons and the atomic core is described by nonlocal and norm-conserving pseudopotentials [23]. Electronic Kohn–Sham wave functions are expanded in a plane-wave basis with a 70 Ryd cut-off. Sums over occupied electronic states are performed by the Gaussian-smearing special-point technique [24, 25], using a Gaussian width of 0.05 Ryd and 60 $\boldsymbol{k}$-points in the irreducible wedge of the BZ. The magnetic moment of Ni is obtained from spin-polarized self-consistent band-structure calculations. Phonon frequencies are calculated on a $(4 \times 4 \times 4)$ regular mesh and Fourier-interpolated in between. This Fourier interpolation amounts to including real-space inter-atomic force constants up to the fourth shell of neighbours. A total of 560 special $\boldsymbol{q}$-points in the irreducible wedge of the BZ are used in the phonon density-of-states (DOS) calculations.

3. Results and discussion

The P–V–T EOS of Ni calculated according to equation (2.2) is shown in figure 1. The ranges of the pressure P and temperature T are from 0 to 80 GPa and from 0 to 800 K, respectively. V_0 (11.16 Å^3) is the equilibrium volume per Ni atom at zero pressure and $T = 298$ K. It can be seen that at a low pressure, the ratio V/V_0 increases significantly as the temperature changes from 50 K to 800 K, which means a large thermal expansion. As the pressure goes higher, the magnitude of the thermal expansion decreases monotonically. When the pressure reaches 80 GPa, we find that the thermal expansion is very small over the whole temperature range from 50 K to 800 K. In figure 2, we compare our calculated results for the P–V relationship (solid line) at $T = 298$ K with the available experimental data [26]. The agreement between the theory and the experiment is excellent over the whole pressure range studied here. We also present the results for three semi-empirical EOSs in figure 2: the dashed line for the Birch [27] EOS, the dotted line for the Murnaghan [28] EOS and the dot–dashed line for the APL (here $L = 2$) EOS proposed by Holzapfel [29]. It can be seen that the Birch model and the APL model work almost as well as the *ab initio* calculations for the system and the pressure range

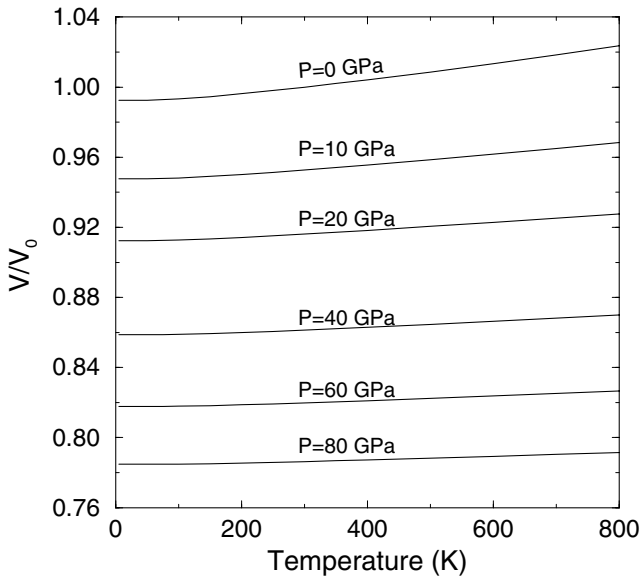

Figure 1. The calculated P–V–T relationship of Ni.

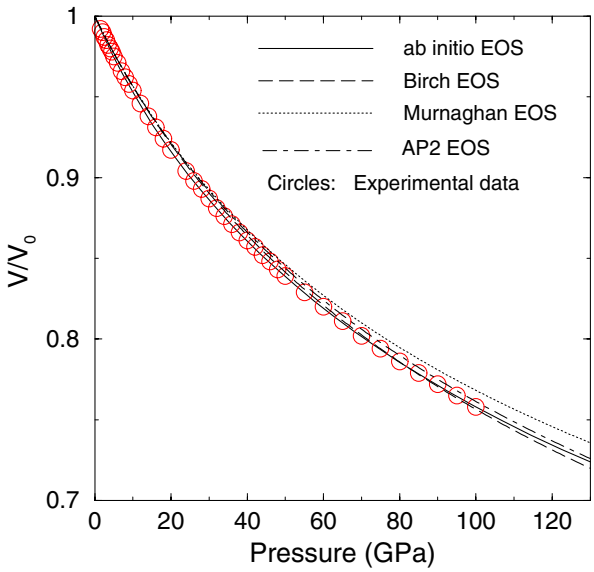

Figure 2. Comparison of the calculated P–V relationship (solid line) at $T = 298$ K with the results of experimental measurement (circles) [26] and from three semi-empirical models.

studied here, while the Murnaghan EOS gives slightly larger volumes at high pressures. It is noted here that we used the same zero-pressure bulk modulus B_0, pressure derivative B_0' and equilibrium volume V_0, obtained by *ab initio* calculations, in the three models and did not treat them as fitting parameters. More extensive studies have shown that the APL model works much better than the Murnaghan model and Birch model in the very high-pressure regions for a lot of systems [29]. The *ab initio* calculations together with the experimental measurements provide a benchmark for checking the validity of different semi-empirical models in the high-pressure region.

Having the EOS to hand, the volume thermal expansion coefficient α_V can be directly derived from equation (2.5). In order to compare with the experimental results, we calculate here the linear thermal expansion coefficient α_L which equals $\alpha_V/3$. Figure 3 shows the variation of α_L with temperature and pressure. The experimental results for α_L at one atmospheric pressure [30] (1 atm $= 1.013 \times 10^{-4}$ GPa) are shown as circles for comparison. It can be seen that at zero pressure, α_L increases exponentially with T at low temperatures and gradually approaches a linear increase at high temperatures. When the pressure increases, the increase of α_L with temperature becomes smaller, especially in the high-temperature range. At a given temperature, α_L decreases drastically with the increase of pressure (figure 3(b)). When the pressure is above 60 GPa, the thermal expansion coefficient α_L at $T = 800$ K is just a little larger than that at $T = 300$ K, which means that the temperature dependence of α_L is pretty small at high pressure. In the meantime, the variation of α_L with pressure also becomes smaller at high pressures.

The B–P–T relationship is shown in figure 4. At fixed pressure P (figure 4(a)), B decreases almost linearly with increasing T, while at a given temperature T (figure 4(b)), B increases almost linearly with P. From the comparison of figure 4(a) and figure 4(b), we can see that the effect of pressure on B is much more significant than that of temperature. The available experimental result [31] (the circle in figure 4(a)) at ambient pressure and room temperature is shown in figure 4(a) for comparison.

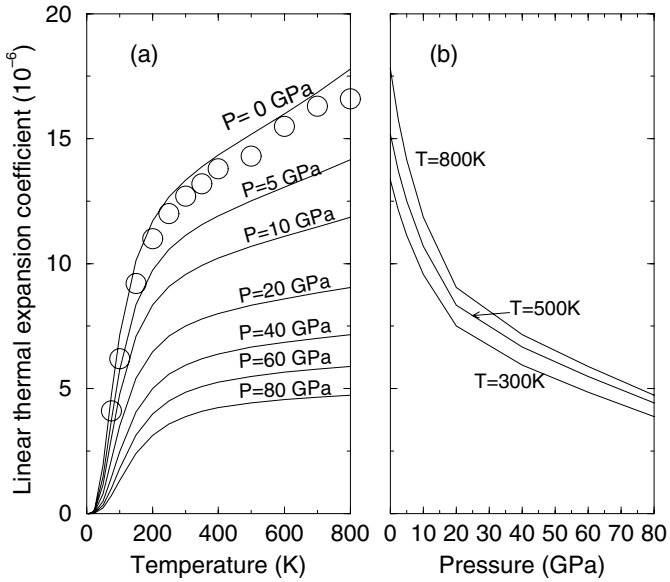

Figure 3. The variation of the linear thermal expansion coefficient α_L with temperature (a) and pressure (b). The available experimental results are shown by circles [30].

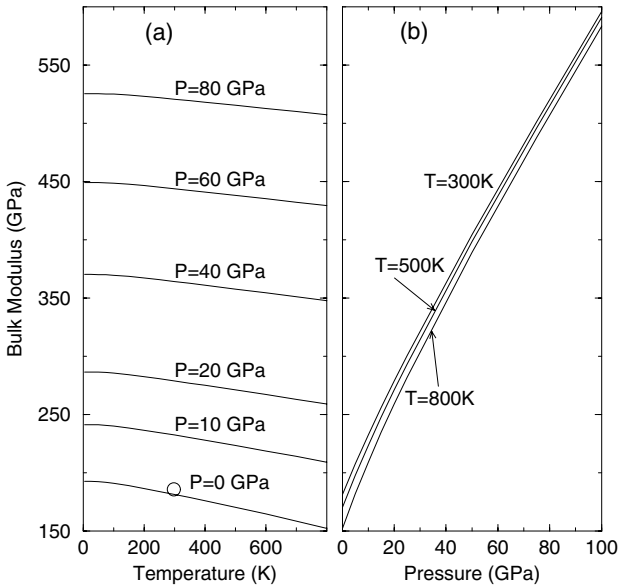

Figure 4. Variation of the bulk modulus of Ni with temperature (a) and pressure (b). The available experimental result [31] is shown by a circle.

The pressure dependence of the phonon dispersion curves of Ni at 298 K is shown in figure 5 and the corresponding variation of the phonon density of states with pressure is shown in figure 6. We can see that the phonon frequencies of Ni in all high-symmetry branches (except for zero frequency at the Γ point) increases with the increase of pressure, which is consistent with the increase of the bulk modulus under pressure (see figure 4). The phonon density of states

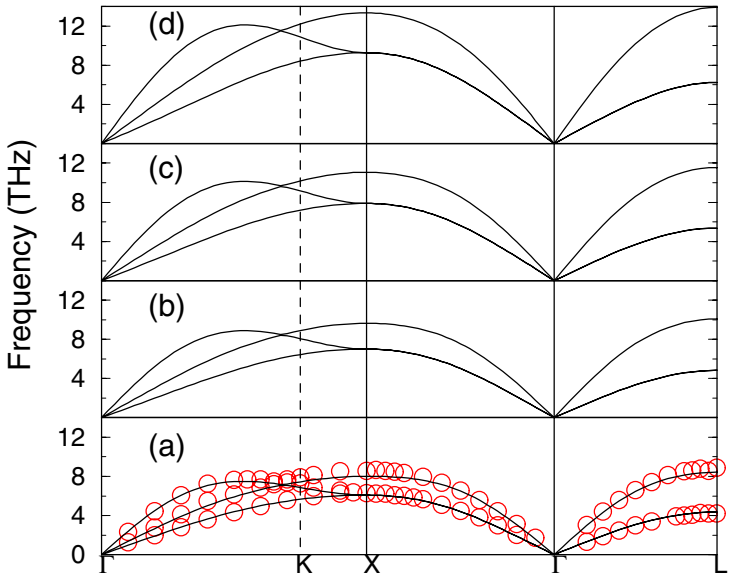

Figure 5. Calculated phonon dispersion curves of Ni at $T = 298$ K. (a) $P = 0$ GPa. Experimental neutron scattering data [32] are denoted by circles. (b) $P = 20$ GPa. (c) $P = 40$ GPa. (d) $P = 80$ GPa.

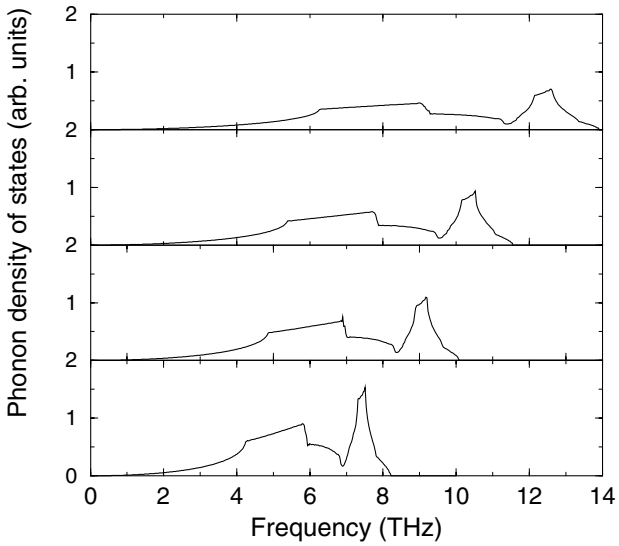

Figure 6. Calculated pressure dependence of the phonon density of states of Ni at $T = 298$ K. (a) $P = 0$ GPa. (b) $P = 20$ GPa. (c) $P = 40$ GPa. (d) $P = 80$ GPa.

spreads up to the high-frequency domain as the pressure increases. Such frequency shifts can be directly detected by high-pressure Raman scattering or neutron scattering experiments. The calculated frequencies at zero pressure are in good agreement with the experimental data [32]. Unfortunately, for the high-pressure results, there are no experimental measurements available for a direct comparison.

The spin-polarized band structures of Ni at different pressures are shown in figure 7 (spin-up bands) and figure 8 (spin-down bands) and the corresponding electronic densities of states (DOS) are shown in figure 9 (spin-up bands) and figure 10 (spin-down bands). The energy zero is set at the Fermi level in figures 7–10. It can be seen that the spin-up d bands are fully filled (in figure 7 and figure 9) while the spin-down d bands are partially filled (in figure 8 and figure 10). Such different numbers of spin-up and spin-down electrons give rise to the net magnetic moment. The energy bands for both spin up and spin down spread downwards as the pressure increases. The corresponding DOS shift downward accordingly. In the meantime, the height of the DOS at the Fermi level (spin-down bands) decreases with pressure which means fewer electronic states at the Fermi level when the pressure is high.

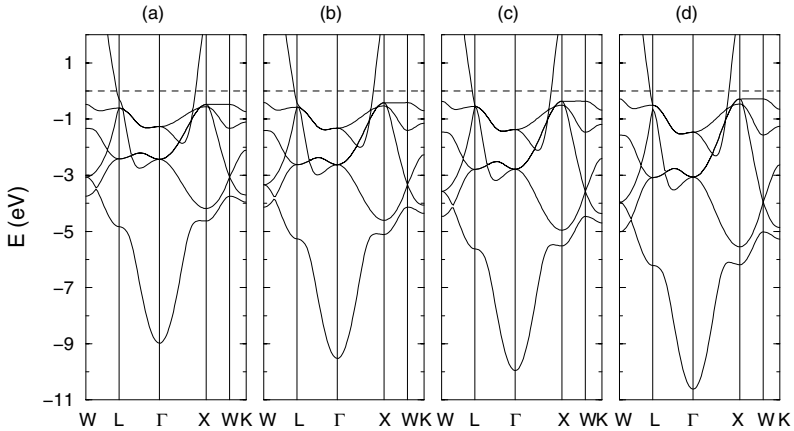

Figure 7. Pressure dependence of the spin-up energy bands of Ni. (a) $P = 0$ GPa. (b) $P = 20$ GPa. (c) $P = 40$ GPa. (d) $P = 80$ GPa.

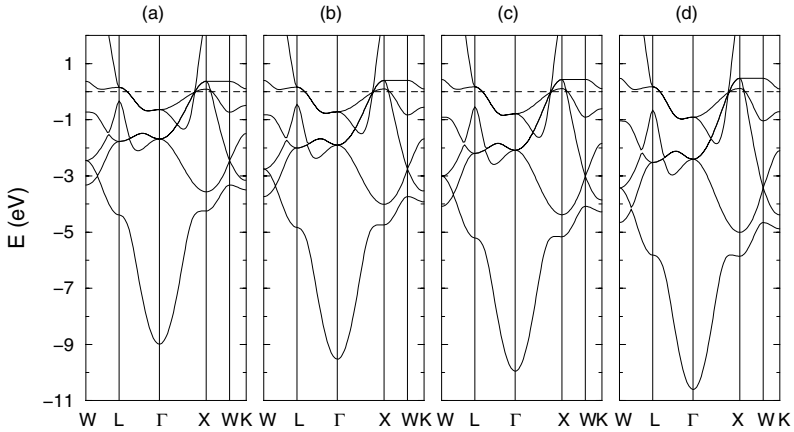

Figure 8. Pressure dependence of the spin-down energy bands of Ni. (a) $P = 0$ GPa. (b) $P = 20$ GPa. (c) $P = 40$ GPa. (d) $P = 80$ GPa.

Figure 11 shows the pressure dependence of the magnetic moment of Ni at 0 K in units of Bohr magnetons (μ_B) per atom. It can be seen that the magnetic moment of Ni decreases monotonically with pressure. At $P = 0$ GPa, the calculated magnetic moment is 0.63 μ_B which is in agreement with the experimental value of 0.62 μ_B [33]. The decrease of magnetic

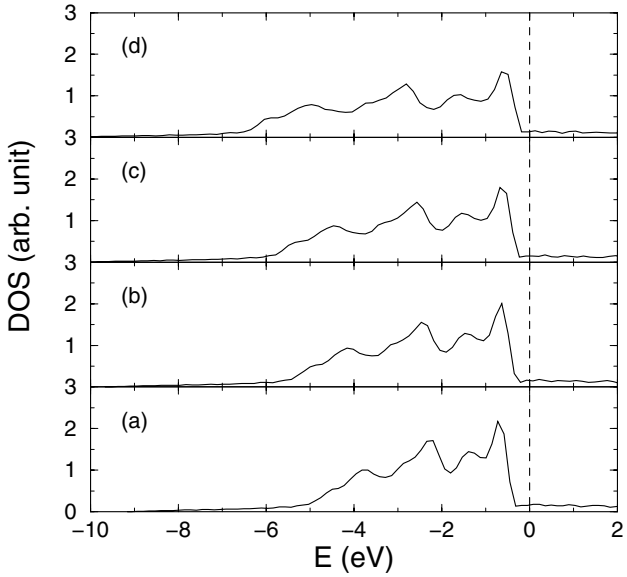

Figure 9. Pressure dependence of the spin-up electronic density of states of Ni. (a) $P = 0$ GPa. (b) $P = 20$ GPa. (c) $P = 40$ GPa. (d) $P = 80$ GPa.

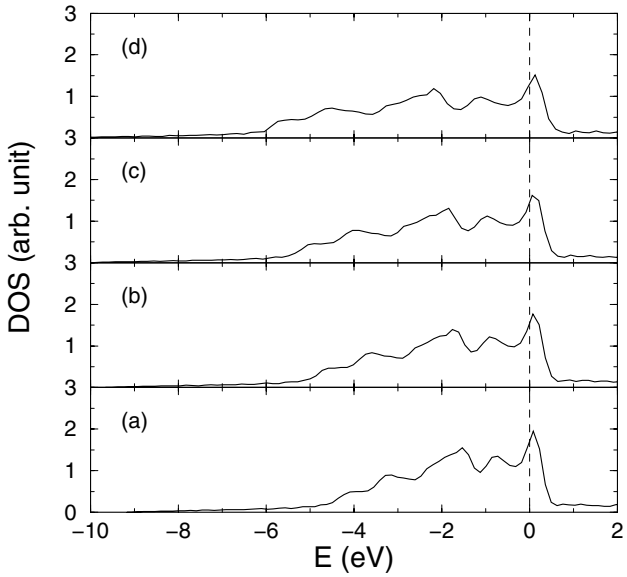

Figure 10. Pressure dependence of the spin-down electronic density of states of Ni. (a) $P = 0$ GPa. (b) $P = 20$ GPa. (c) $P = 40$ GPa. (d) $P = 80$ GPa.

moment with pressure indicates a weak ferromagnetism of Ni at high pressures. In order to characterize the variation trend of the magnetic moment (M) of Ni with pressure, we fit the calculation results using a simple formula: $M(P) = M_0 + \alpha P + \beta P^2$. The values obtained for α and β are -1.18×10^{-3} μ_B GPa^{-1} and 6.8×10^{-6} μ_B GPa^{-2}, respectively. This formula can be easily used and checked in other high-pressure studies.

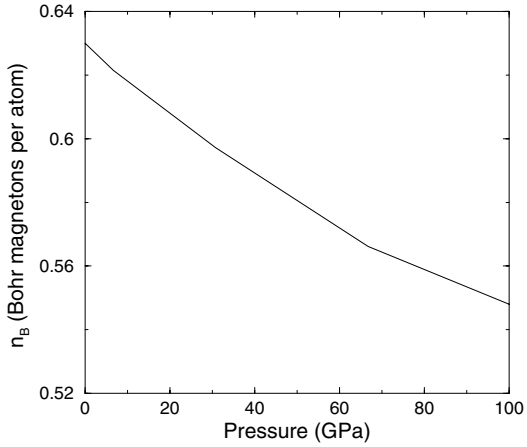

Figure 11. Pressure dependence of the magnetic moment of Ni.

4. Summary

In this study, we have calculated the thermodynamic, electronic and magnetic properties of Ni, using the quasiharmonic approximation within the density-functional theory. The *equation of state* is constructed from the *ab initio* Helmholtz free energy. The volume dependence of the phonon frequencies is calculated from the density-functional perturbation theory. It is found that the high pressure results in a smaller thermal expansion coefficient, a larger bulk modulus, higher phonon frequencies and smaller magnetic moment. The results obtained for the quantities investigated are in good agreement with the available experimental measurements. Comparing with the experimental data and *ab initio* calculations, it is found that the Birch EOS gives a better description of the P–V relationship of Ni under high pressures than the Murnaghan EOS does. We also give a simple relationship between the magnetic moment of Ni and the external pressure.

Acknowledgment

This work was supported by the Department of Energy (DOE) under the contract W-7405-ENG-36.

References

[1] Munro D C 1963 *High Pressure Physics and Chemistry* ed R S Bradley (London: Academic) ch 2, pp 11–49
[2] Jayaraman A 1983 *Rev. Mod. Phys.* **55** 65
[3] Miller G H and Ahrens T J 1991 *Rev. Mod. Phys.* **63** 919
[4] Holzapfel W B 1997 *High-Pressure Techniques in Chemistry and Physics* ed W B Holzapfel and N S Isaacs (Oxford: Oxford University Press)
[5] Hama J and Suito K 1996 *J. Phys.: Condens. Matter* **8** 67 and references therein
[6] Parrinello M and Rahman A 1982 *J. Chem. Phys.* **76** 2602
[7] Focher P, Chiarotti G L, Bernasconi M, Tosatti E and Parrinello M 1994 *Europhys. Lett.* **36** 345
[8] Allen R E and de Wette F W 1969 *Phys. Rev.* **179** 873
[9] Baroni S, Giannozzi P and Testa A 1987 *Phys. Rev. Lett.* **58** 1861
[10] Giannozzi P, de Gironcoli S, Pavone P and Baroni S 1991 *Phys. Rev.* B **43** 7231
[11] Foiles S M and Adams J B 1989 *Phys. Rev.* B **40** 5909

[12] Xu C H, Wang C Z, Chan C T and Ho K M 1991 *Phys. Rev.* B **43** 5024
[13] Althoff J D, Allen P B, Wentzcovitch R W and Moriarty J A 1993 *Phys. Rev.* B **48** 13 253
[14] Barrera G D, Taylor M B, Allan N L, Barron T H K, Kantorovich L N and Mackrodt W C 1997 *J. Chem. Phys.* **107** 4337
[15] Biernacki S and Scheffler M 1989 *Phys. Rev. Lett.* **63** 290
[16] Fleszar A and Gonze X 1990 *Phys. Rev. Lett.* **64** 2961
[17] Pavone P, Baroni S and de Gironcoli S 1998 *Phys. Rev.* B **57** 10 421
[18] Quong A A and Liu A Y 1997 *Phys. Rev.* B **56** 7767
[19] Xie J J, de Gironcoli S, Baroni S and Scheffler M 1999 *Phys. Rev.* B **59** 965
[20] Xie J J, Chen S P, de Gironcoli S and Baroni S 1999 *Phil. Mag.* B **79** 911
[21] Brüsch P 1982 *Phonons: Theory and Experiments I* (Berlin: Springer)
[22] Perdew J P and Wang Y 1992 *Phys. Rev.* B **45** 13 244
[23] Hamann R 1989 *Phys. Rev.* B **40** 2980
[24] Monkhorst H J and Pack J D 1976 *Phys. Rev.* B **13** 5188
[25] Methfessel M and Paxton A T 1989 *Phys. Rev.* B **40** 3616
[26] Kennedy G C and Keeler R N 1972 *American Institute of Physics Handbook* 3rd edn (New York: McGraw-Hill) section 4, p 101
[27] Birch F 1967 *J. Geophys. Res.* **72** 3661
[28] Murnaghan F D 1944 *Proc. Natl Acad. Sci. USA* **30** 244
[29] Holzapfel W B 1998 *High Pressure Res.* **16** 81
[30] Gray D E (ed) 1963 *American Institute of Physics Handbook* 2nd edn (New York: McGraw-Hill) pp 4–66
[31] Kittel C 1986 *Introduction to Solid State Physics* 6th edn (New York: Wiley)
[32] De Wit G A and Brockhouse B N 1968 *J. Appl. Phys.* **39** 451
[33] Frederikse H P R 1998 *Handbook of Chemistry and Physics* ed D R Lide (Boca Raton, FL: Chemical Rubber Company Press) pp 12–117